THE 1984 SOLAR OSCILLATION PROGRAM OF THE MT. WILSON 60-FOOT TOWER

Edward J. Rhodes, Jr.
Department of Astronomy
University of Southern California
Los Angeles California 90089
and
Space Physics and Astrophysics Section
Jet Propulsion Laboratory
California Institute of Technology
Pasadena, California 91109

Alessandro Cacciani
Department of Physics
University of Rome
Rome, Italy

Steven Tomczyk and Roger K. Ulrich
Department of Astronomy
University of California at Los Angeles
Los Angeles, California 90024

ABSTRACT. We describe here the instrumentation, data, and preliminary results from the summer, 1984, solar oscillation observing program which was carried out using the 60-foot tower telescope of the Mt. Wilson Observatory. This program was carried out with a dedicated solar oscillation observing system and obtained full-disk Dopplergrams every 40 seconds for up to 11 hours per day. Between June and September, 1984, observations were obtained with a Na magneto-optical filter on 90 different days. The data analysis has progressed to the point that spherical harmonic filter functions have been employed to generate a few one-dimensional power spectra from a single day's observations.

1. INTRODUCTION

Shortly after the initial observations of high-degree solar p-mode oscillations (Deubner, 1975; Rhodes, Ulrich, and Simon, 1977; Deubner, Ulrich, and Rhodes, 1979) two of us (EJR and RKU) recognized the need for a dedicated solar oscillation observing system. Accordingly, we began to develop such a system jointly with Dr. Robert F. Howard at the Mt. Wilson Observatory. The initial design of this system was developed during 1978 and major modifications were made to

this design during 1980 and 1981. The two most significant improvements were the replacement of one-dimensional Reticon detectors with a CID camera system, and the use of a magneto-optical filter instead of a spectrograph. The developmental status of this system was first described by Rhodes et al. (1981). More recent reports about this system were given by Rhodes et al. (1983 and 1984a). The first solar oscillation power spectrum obtained with this system during July, 1983, was presented in Rhodes et al. (1984a and 1984b).

Here we wish to report on the first extended operation of this oscillation system in the manner for which it was orginally designed: the acquisition of daily full-disk Dopplergrams with high time resolution. During the fall of 1983 and the spring of 1984 the full-disk imaging capability of the system was installed and tested with the goal of obtaining such observations throughout the 1984 observing season. We will first report on the observations which were obtained and then finish with a progress report on the status of the reduction of that data. The analysis of a larger quantity of this data is currently in progress with our primary goals being an improvement in the published accuracy of low- and intermediate-degree p-mode frequencies and the probing of solar internal rotation as functions of depth and latitude as Brown has reported earlier at this meeting (Brown, 1985).

2. OBSERVATIONS

The observations obtained during the summer of 1984 consisted of pairs of narrow-band filtergrams which were obtained in the two Na D lines. The filtergrams were obtained with a two-cell version of the magneto-optical filter (MOF) which was originally invented by Cacciani. This filter was first described in Cimino et al. (1968a and 1968b), and in Cacciani et al. (1970). Its uses for solar observations were later described in Agnelli, Cacciani, and Fofi (1975); in Cacciani and Fofi (1978); in Cacciani, Fortini, and Torelli (1980); and in Cacciani et al. (1981). More recently, its principles of operation were reviewed by Cacciani and Rhodes (1984), who described both one-and two-cell versions of it.

Figure 1 shows the two-cell configuration of the MOF which was employed during May through September, 1984, to obtain the data described here. During that time the filter employed two 1000-Gauss permanent magnets. (Subsequent to September, 1984, the first of these two magnets was replaced with a 6000-Gauss permanent magnet and this combination of 6000- and 1000-Gauss magnets has been adopted for all subsequent Na observations.)

At the left of the magnets in Figure 1 we show the mechanism which controlled the moveable quarter-wave plate. This mechanism consisted of a reversible stepper motor and a Geneva movement. When operated under the control of an LSI-11 microcomputer, this mechanism allowed us to rotate the wave plate through angles of +45° and -45°

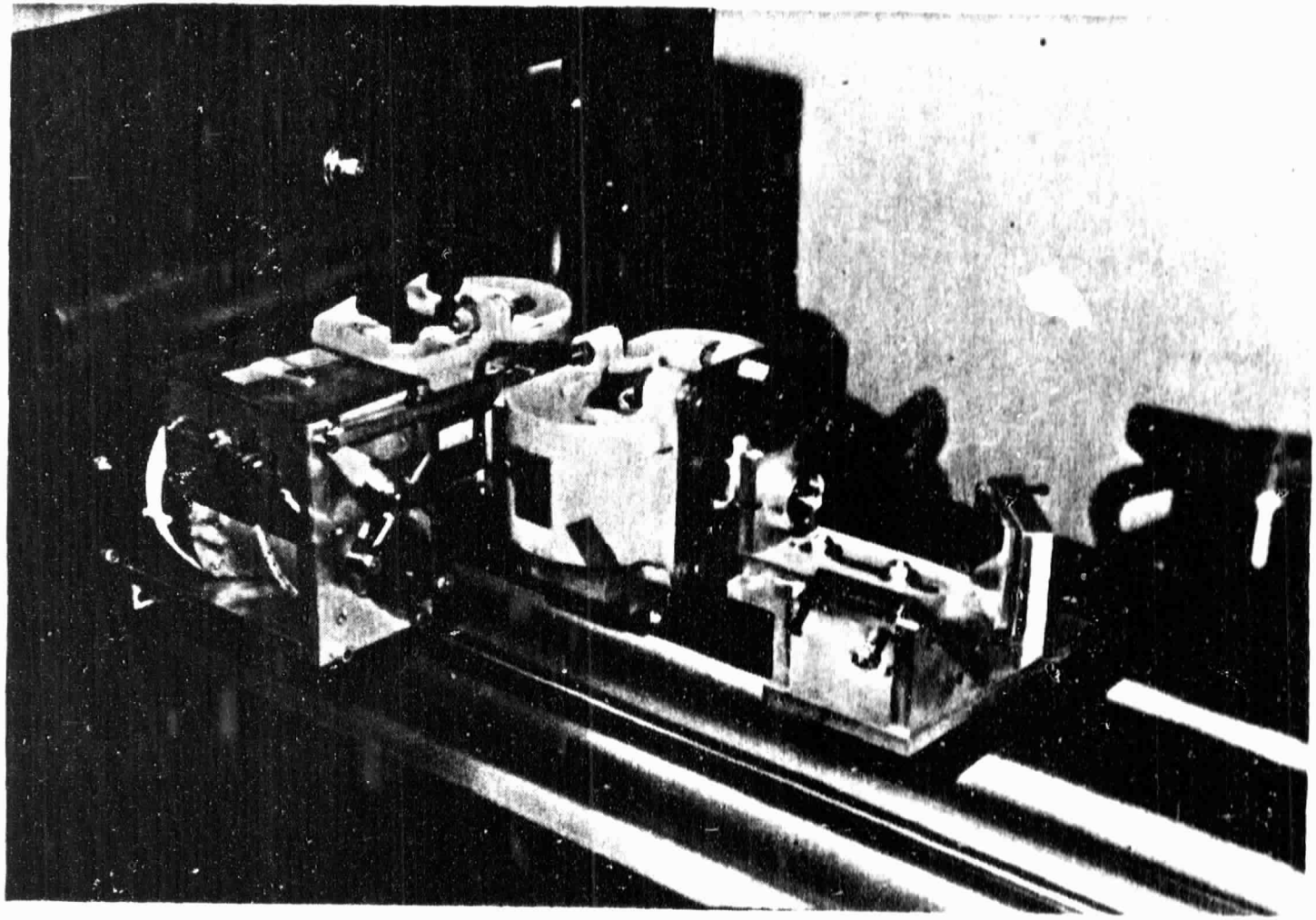

Figure 1. Magneto-Optical Filter. This figure shows the two-cell Na MOF as it was installed at Mt. Wilson during 1984. At that time the filter employed two 1000-Gauss magnets.

with respect to the crossed polarizers which were also part of the MOF.

When the wave plate was positioned in the +45° position, for example, we were able to record filtergrams in the bandpass located on the red side of the NaD lines, while a rotation of the wave plate to the -45° angle tuned the filter to the blue bandpass.

The exposures of the Photometrics, Ltd. CID camera which we employed were regulated by a rotating disk shutter. The rotation of this shutter was governed by a series of uniformly-spaced stepper motor pulses which were supplied to the shutter by a Superior Electronic Buffered Translator. Each filtergram took 5 seconds for both exposure and camera read-out and so a pair of red- and blue-wing filtergrams could have been obtained once every 10 seconds. In fact, this sequence was only repeated once every 40 seconds for up to 11.4 hours per day. Therefore, a single day's observing run consisted of a maximum of 1024 red filtergrams and 1024 blue filtergrams.

The transmission profiles of the two-cell MOF were similar to those shown in Figure 2. Here we show two more-recent prfiles which were obtained in the NaD1 line with the 6000-Gauss/1000-Gauss combination of magnets mentioned earlier. These wavelength scans were obtained with the spectrograph of the 150-foot tower telescope at Mt. Wilson. The two profiles corresponding to the +45° and -45° positions of the quarter-wave plate are superimposed upon each other in this Figure. The degree of separation of the two bandpasses is illustrated by the low level of the transmission of each curve at the location of the peak of the other curve.

The cumulative amount of data obtained during our 1984 campaign is shown in Figure 3. Here the number of hours of cloud-free observations obtained on each day is plotted as a function of time. The initial observations were obtained on May 8, while the last observations were obtained on September 9. The stipled portion of the diagram shows that most of the May data was subsequently destroyed when all but the first one of each day's tapes were later re-written with newer data in early August. A single tape per day from that period was saved in order to have some Dopplergrams for eventual comparison with those produced at the 150-foot tower on the same days. On some of the days between May 20 and June 8 several other tests were run with the MOF and with the observing hardware; hence, the absence of data during that interval was not due to a period of bad weather.

Figure 3 shows that on several occasions during the campaign we did indeed obtain 7 to 11 hours of cloud-free data per day for intervals exceeding one week in duration. On only 12 days after with June 24 was the weather bad enough to prevent the recording of any data at all. The fact that this much data was obtained during 1984 was due solely to the diligence of S. Tomczyk who observed and archived

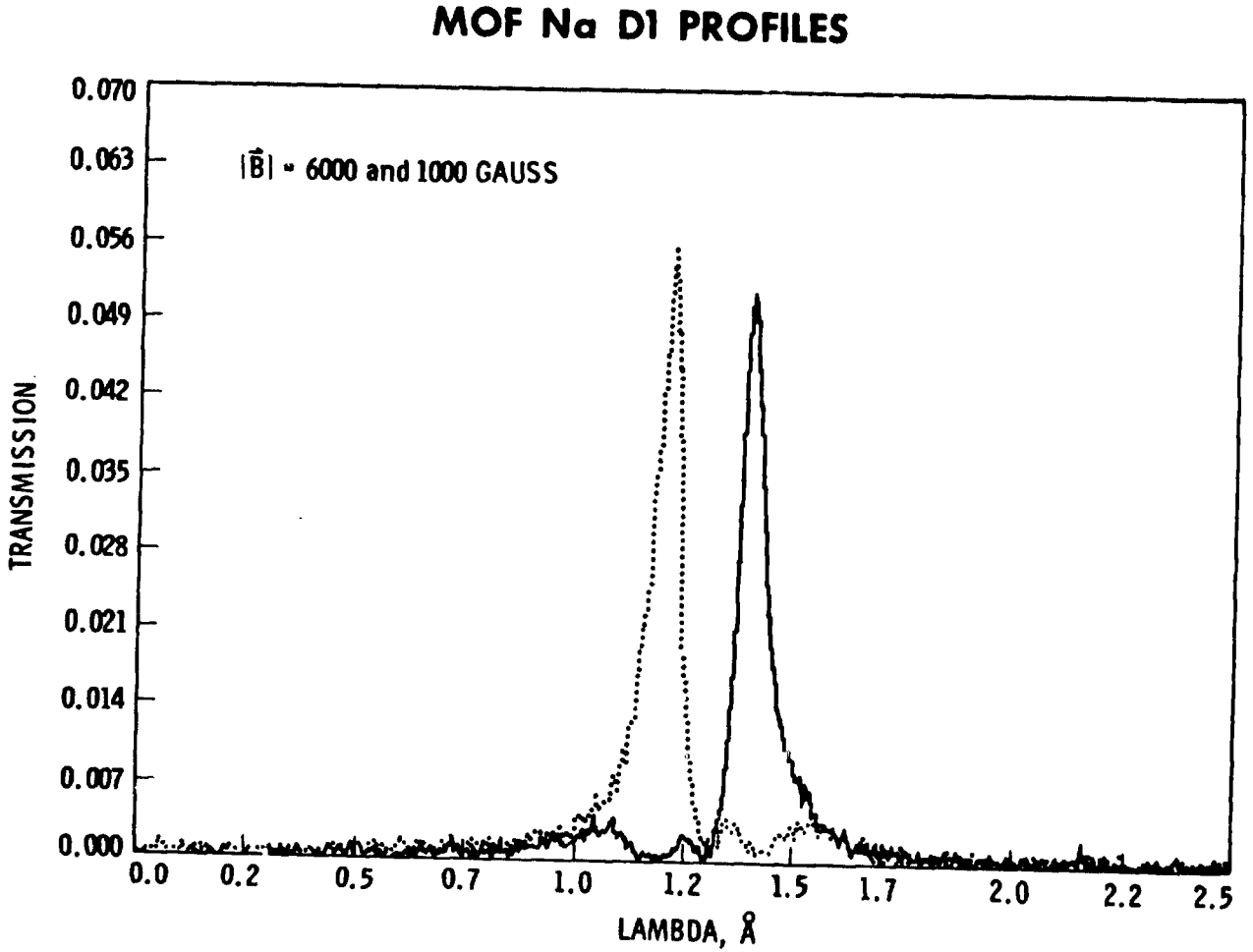

Figure 2. Magneto-Optical Filter Transmission Profiles. The red- and bluewing Na D1 transmission profiles for a two-cell MOF are shown. The magnetic field strengths were 6000 Gauss and 1000 Gauss, in cells 1 and 2, respectively. The input power was 25.0 watts in cell 1 and 14.5 watts in cell 2.

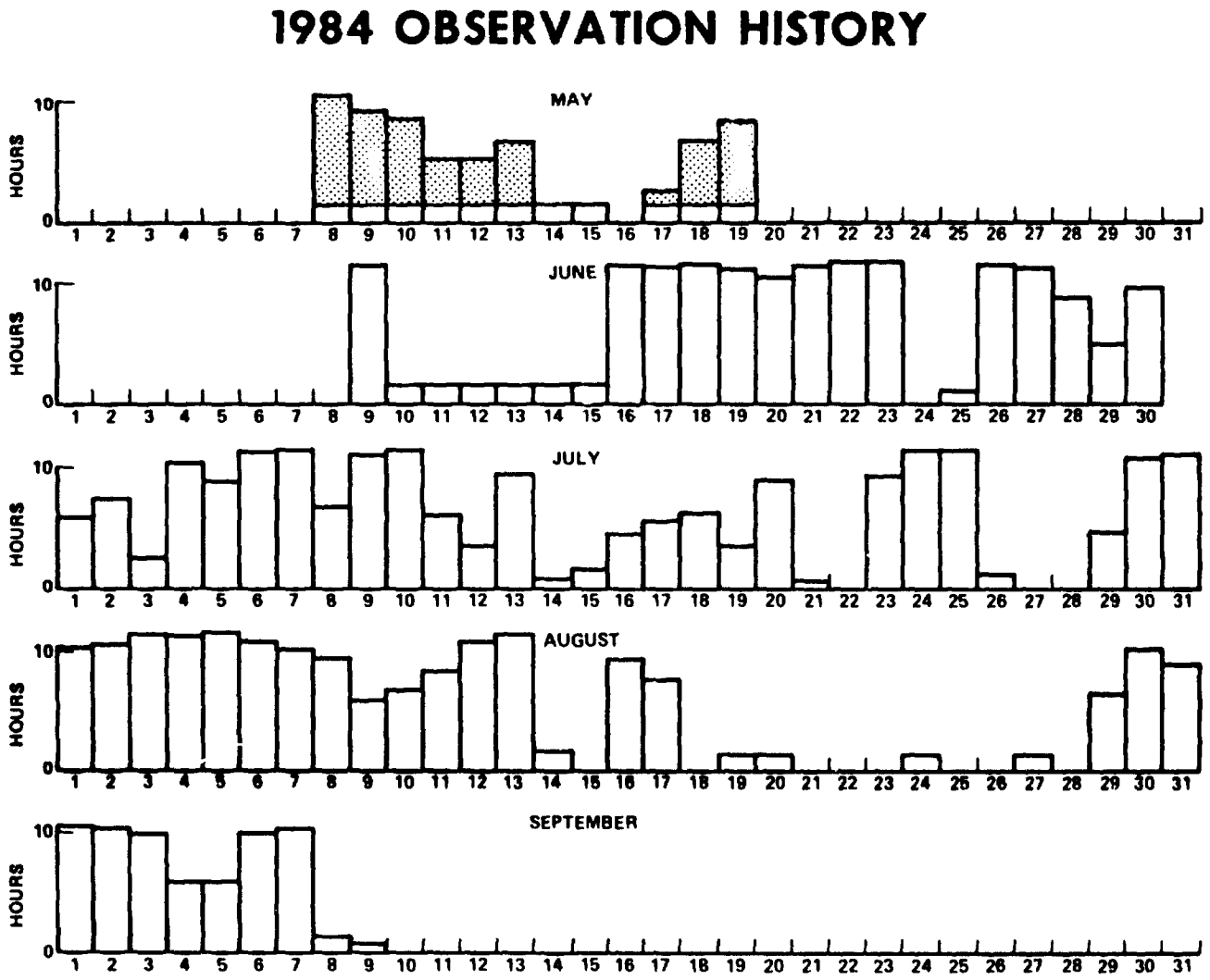

Figure 3. Observational History. The number of hours of data obtained each day is plotted as a function of time during May-September 1984.

the data almost single-handedly for the entire three months.

A histogram of the number of days having a given length run is shown in Figure 4. Inspection of this figure shows that on 45 of the 90 days at least 8 hours of data was obtained. Since this histogram only includes the number of cloud-free hours on each day, the total amount of data that was obtained actually exceeded the amount shown in the histogram. The large number of days having between one and two hours of data was the result of our effort to record at least a single tape's worth of data even when it became obvious early in a given day that the weather would not permit the full-day run to be completed.

3. CONVERSION INTO DOPPLERGRAMS

At the conclusion of each day's observations the time series of alternating red and blue filtergrams was archived from disk to tape. The first steps in the analysis of this data were the computation of the location of the disk center of each filtergram and the translational registration of each filtergram to a common center location. The registration process was necessary to correct for the image motion which occurred between the acquisition of each red filtergram and its corresponding blue companion. It also allowed us to correct for slow drifts in the solar image introduced by the guider on the time scale of several hours.

After the filtergrams were registered in the computer, each pair could then be converted into a Dopplergram with the following simple formula:

$$\text{velocity } (x,y) = \text{constant}^* \frac{I_{blue}(x,y) - I_{red}(x,y)}{I_{blue}(x,y) + I_{red}(x,y)} \qquad (1)$$

where I_{blue} and I_{red} referred to the intensities of the pixel at location (x,y) in the blue and red filtergrams and the constant was a calibration constant which had to be determined in some way.

A Dopplergram similar to those employed with the 244x248 pixel CID camera and the Na MOF is shown here in Figure 5. The figure shows a Dopplergram which was obtained with a JPL 800x800 pixel CCD camera (although only an area 500 pixels on a side was employed in this instance). This Dopplergram was obtained on June 1, 1984. It was obtained by differencing two filtergrams which were taken 15 seconds apart; hence, the appearance of the solar limb is due to slight image distortions caused by the Earth's atmosphere during and between the exposure of the two filtergrams. Solar rotation is visible as the shading from white to black across the visible disk.

By comparison we show the Dopplergram obtained in λ5250 with

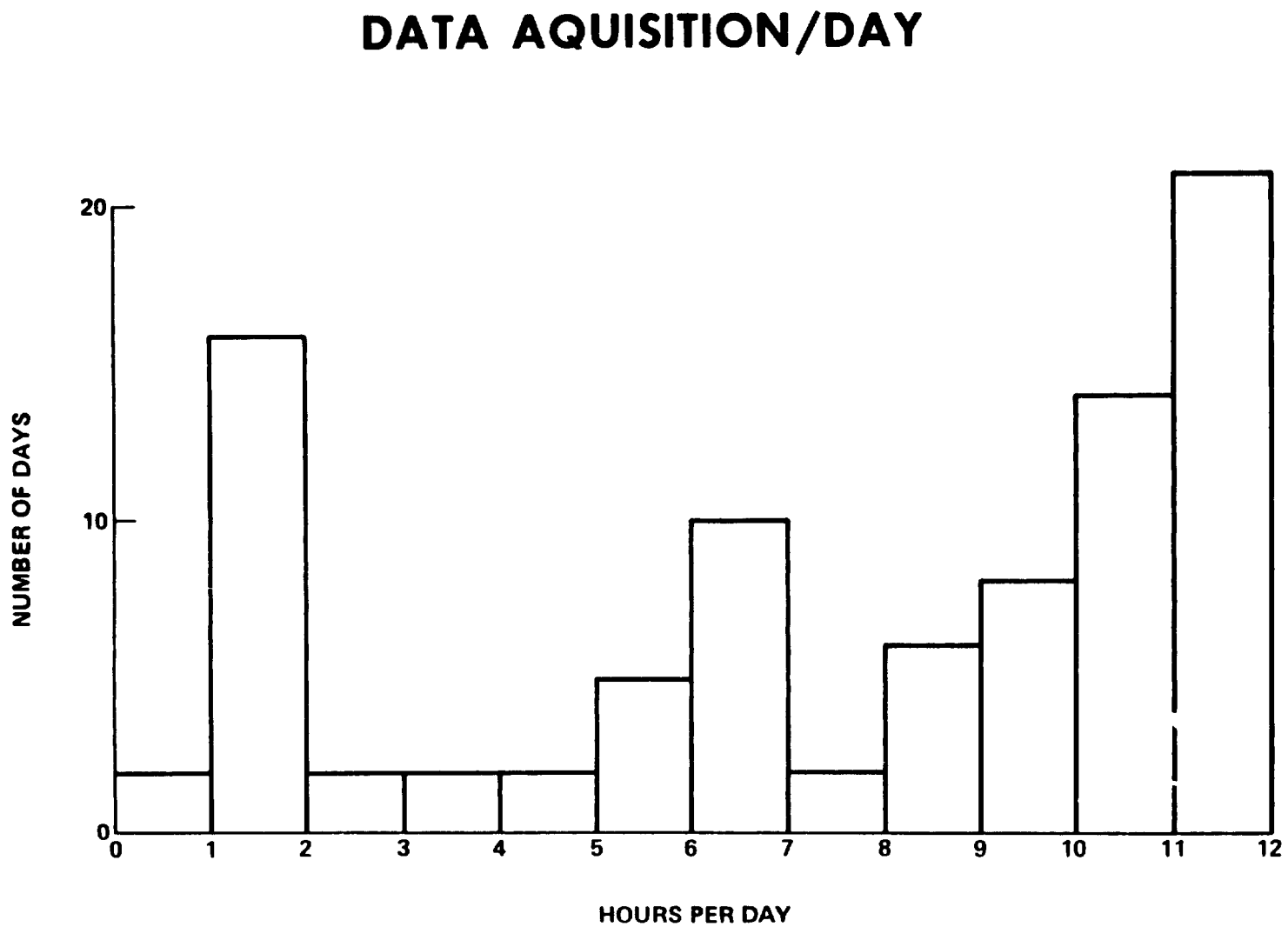

Figure 4. Mean Acquisition Histogram. The number of days having a given run length are plotted as a function of observing run length.

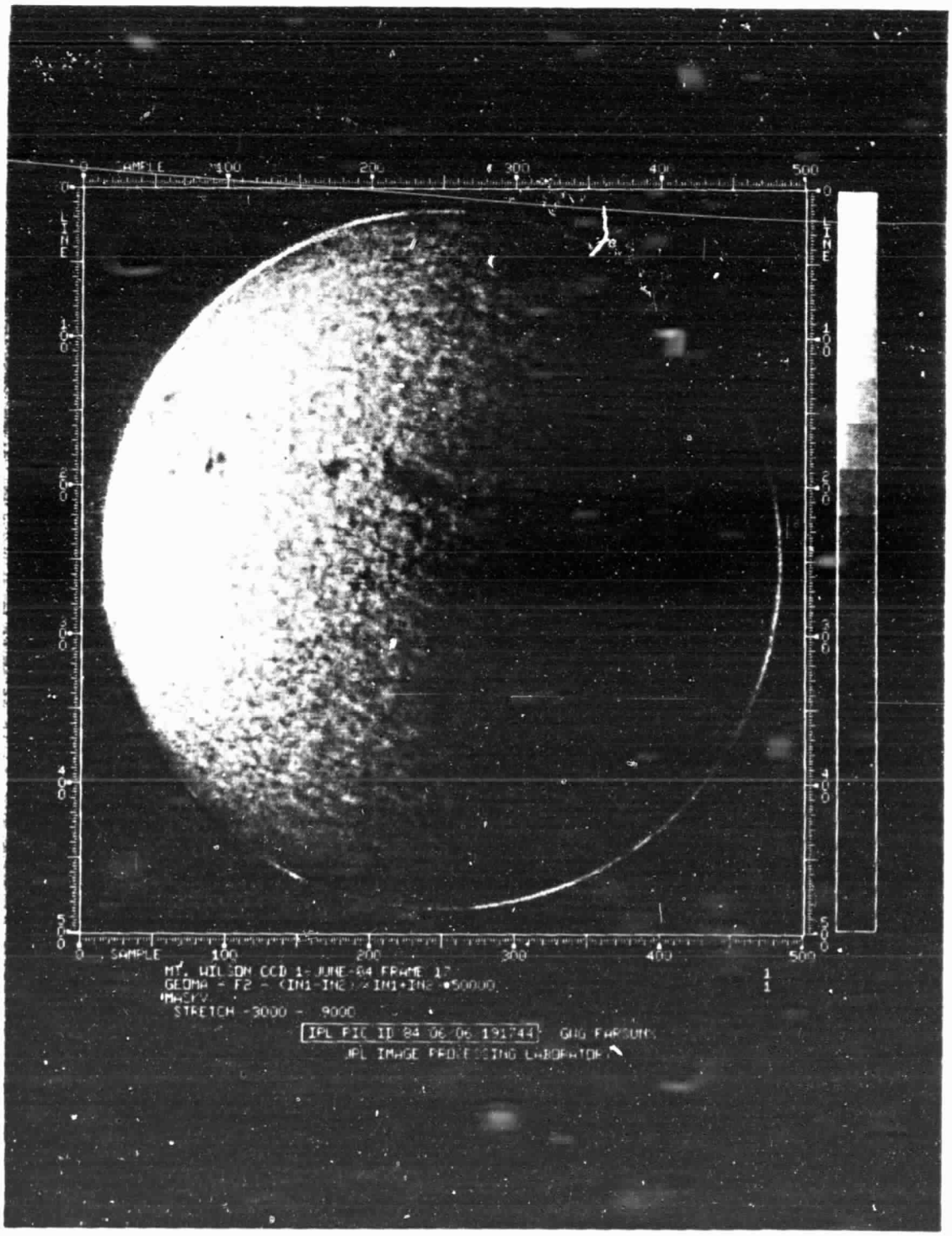

Figure 5. MOF Dopplergram. Na Dopplergram obtained with MOF and 800x800 pixel CCD camera on 1 June 1984. Solar rotation is visible as the shading across the disk.

the spectrograph of the 150-foot tower on the same day in Figure 6.

Again, solar rotation is visible across the disk as are several active regions.The velocity flows around the active regions are less pronounced in the λ5250 Dopplergram than they were in Figure 5. Some of this difference may be due to the fact that the NaD lines are chromospheric lines while λ5250 is a photospheric line. Additional tests at Mt. Wilson will be needed to clarify this possibility.

The constant given in equation (1) can in principle be determined in two different ways and hence confirmed independently. First, it is possible to use the rate of solar rotation as measured in a particular latitude zone on a given day at the 150-foot tower to provide the radial velocities against which the observed intensity differences can be compared. The idea is illustrated schematically in Figure 7. Here the scaled Doppler signal (defined for now as $50000 \cdot [I_B - I_R]/[I_B + I_R]$) from a full-disk Dopplergram obtained with the CID camera is shown as a function of position along a swath that was located parallel to the solar equator. If the MOF were responding linearly to the solar radial velocity over a range of ± 200 m/sec, then we would expect to see a perfectly straight line running from one end of the equator to the other, while the slope of this straight line would be related to the solar rotational velocity. That is, for the 150-foot tower Dopplergram of Figure 6, a slope of roughly 2 m/sec/arcsecond would be obtained near the equator.

A regression analysis of the so-called Doppler signal against the measured solar velocities along the equator would then yield a straight line whose slope could later be used to convert a particular intensity difference anywhere on the disk into an equivalent radial velocity. The degree of constancy of this calibration constant over the solar image would then be a measure of the presence or absence of systematic velocity errors introduced by the MOF. The principal objection to employing this calibration method is that it makes use of the 150-foot tower Dopplergrams to provide measurements of the very quantity which the MOF is trying to measure, namely, the solar radial velocity at each point on the visible disk.

An alternative calibration procedure is to compute an average Doppler signal for every single Dopplergram and to then compute what the predicted Earth-sun radial velocity was for the moment in time. This later calculation can be made with an ephemeris program and subsequently a regression analysis can be carried out of these Doppler signals as a function of the predicted velocity. The slope and intercept of the regression line that is so obtained will then be the calibration constants necessary for conversion of the intensity differences into radial velocities.

Two different applications of this latter approach are illustrated here in Figures 8 and 9. In the upper left panel of Figure 8 we have plotted the mean Doppler signal ($10000\ [I_B-I_R \cdot [I_B+I_R]$) which

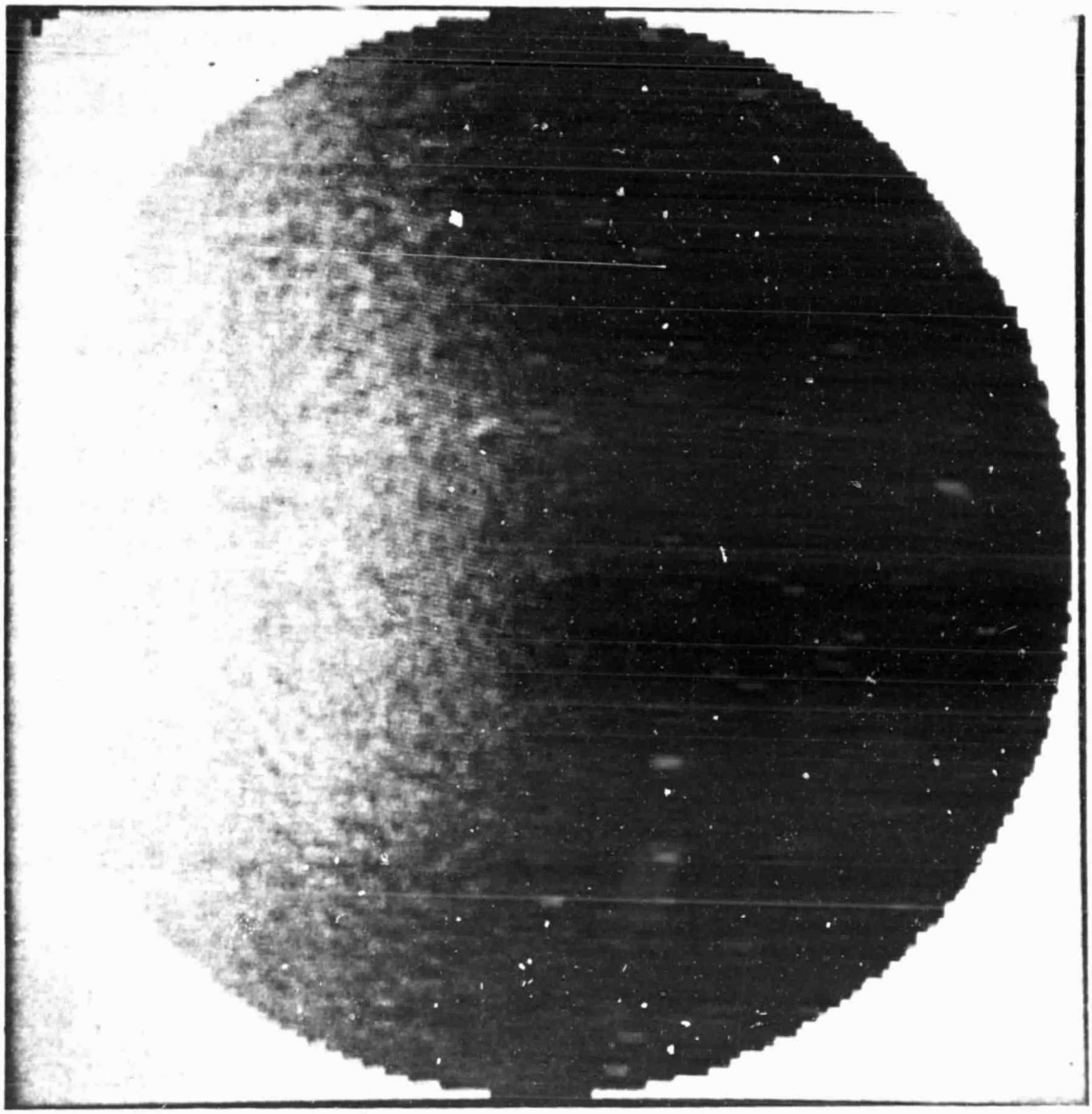

Figure 6. Comparison Dopplergram. A Dopplergram obtained in λ5250 with the spectrograph at the Mt. Wilson 150' tower telescope on 1 June 1984.

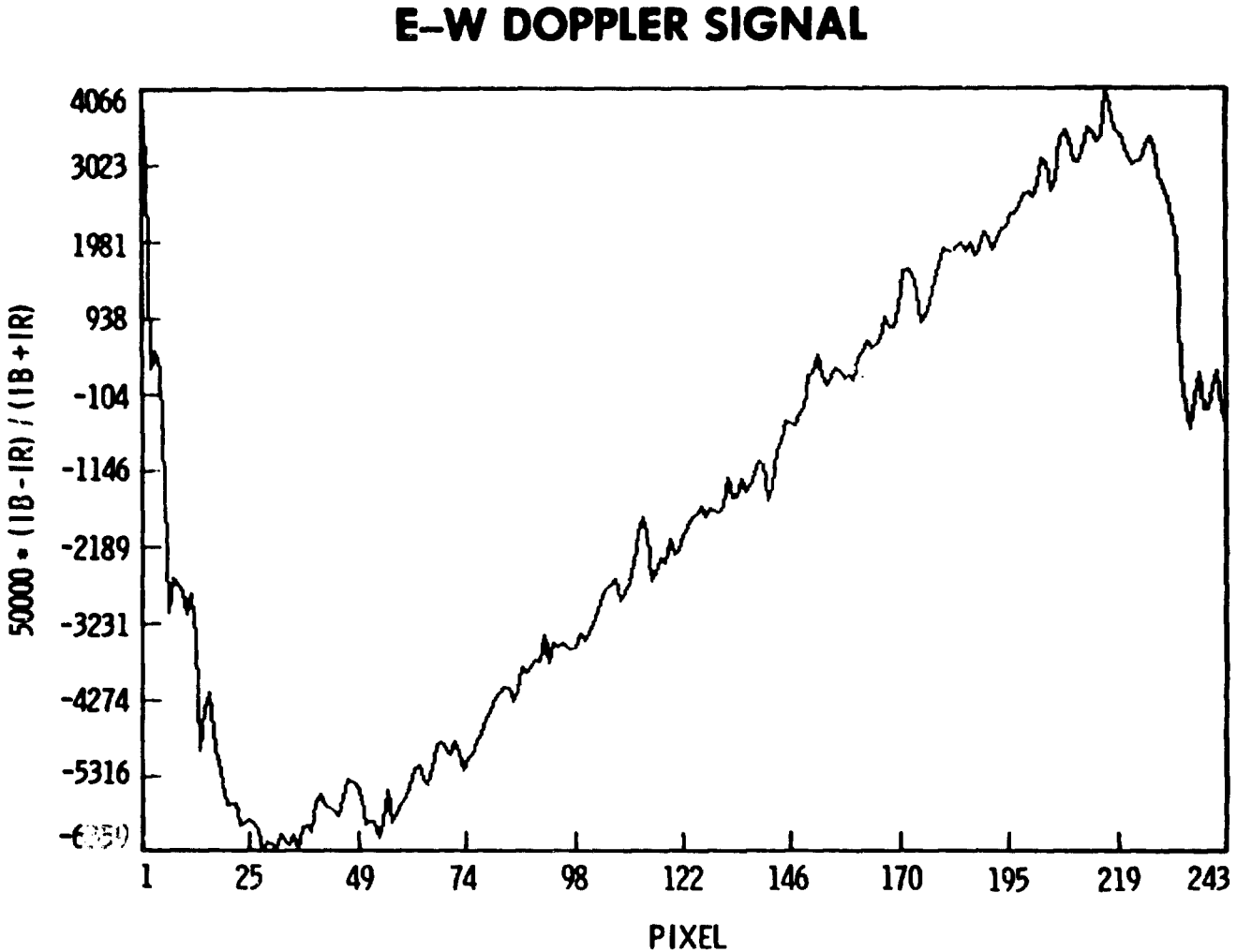

Figure 7. East-West Doppler Signal Profile. The Doppler signal (50000 • [IB-IR]/[IB+IR]) from a full-disk Dopplergram obtained with the CID camera is shown as a function of position along a swath parallel to the solar equator. Solar rotation is responsible for the slope of the profile.

we obtained by averaging the raw Doppler signal from individual pixels within a 512" x 512" area at the center of the solar disk. Here this mean Doppler signal is shown as a function of the Universal time at which each frame of data was recorded.

In the upper right panel of Figure 8 we have plotted the radial velocity of the Earth relative to the sun as a function of Universal Time. The radial velocities shown in the panel were computed with an emphemeris program which was originally developed at JPL for the interplanetary program, and which includes the effects of planetary perturbations on the Earth. The output from this JPL program was combined with computations of the Earth's diurnal motion and of the Earth's lunar barycentric motion in order to provide the total radial velocity between Mt. Wilson and the sun at every moment of time. The rotation of the Earth is clearly visible in this panel.

In the bottom panel we have plotted the mean Doppler signal versus the corresponding computed sun-Earth velocity for that moment of time.A linear regression analysis was performed upon the data shown in this panel and we obtained the regression coefficients listed at the top of the Figure. The slope of 1.222 m/sec per Doppler unit is what would later be used to convert individual pixel difference signals into radial velocities. The intercept of the regression line includes the effects of: 1) the gravitational redshift, 2) asymmetries in the solar line profile, and 3) asymmetries in the transmission profile of the MOF, as were seen in Figure 2. The correlation coefficient of 0.993 from the regression analysis shows that the Doppler/velocity conversion was indeed quite linear for this particular data.

The MOF data used to generate Figure 8 were obtained in July 1983.When we repeated this analysis with the 1984 full-disk data described in Section 2, we got the results shown in Figure 9. Here the mean Doppler signal shown in the upper left panel was obtained by averaging the Doppler signal over the entire visible disk of the sun. Again the computed sun-Earth radial velocities for the observing times of each frame are plotted at the upper right. And again, at the bottom, we show the results of plotting the mean Doppler signal against the computed radial velocity. Here the relationship is not nearly as linear as was that shown in Figure 8. While we are not yet certain of the cause of this departure from linearity, we have noticed that the discrepancy is worst at large hour angles early in the morning and late in the afternoon. Thus, we currently believe that telluric H_2O contamination in the wings of the NaD2 line, which would have the greatest effect at the largest air masses, may be introducing the time-dependent departure from linearity which we are seeing in Figure 9. We will repeat this type of analysis for every day's worth of data in order to see whether or not this departure from linearity is always present in the 1984 data. (In the meantime, we have observed only in the D2 line during 1985 since that line has much less telluric contamination.)

REGRESSION ANALYSIS

Y-INT: -.11695D+04 +/- .42635D+01 M/SEC
SLOPE: .12222D+01 +/- .48351D-02 M/SEC / VEL UNITS
R: .99304D+00

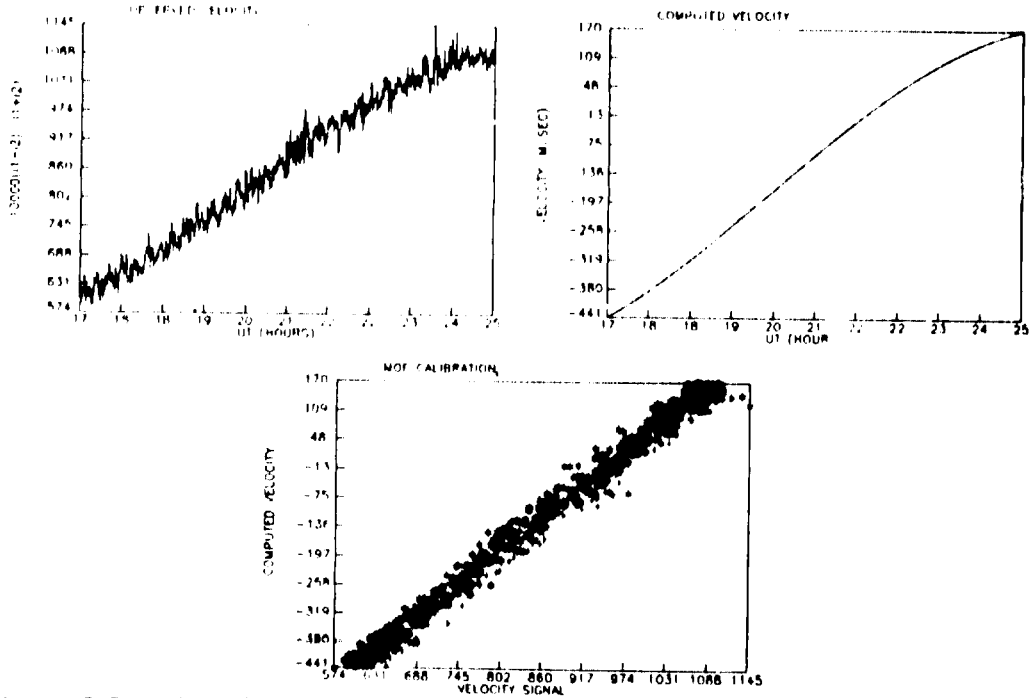

Figure 8. Calibration of Doppler Signal. This figure shows how the rotation and orbital motion of the Earth can be used to calibrate the MOF's Doppler signal. In the upper left the Doppler signal obtained by averaging over a 512" x 512" area at the center of the solar disk is displayed as a function of Universal Time. In the upper right the radial velocity of the Earth relative to the sun as computed from an ephemeris program is also displayed versus versus Universal Time. At the bottom the computed velocity is plotted against the average Doppler signal for the corresponding moments of time. The linear regression analysis shows that the two quantities are linearly related with a correlation coefficient of 0.993.

REGRESSION ANALYSIS

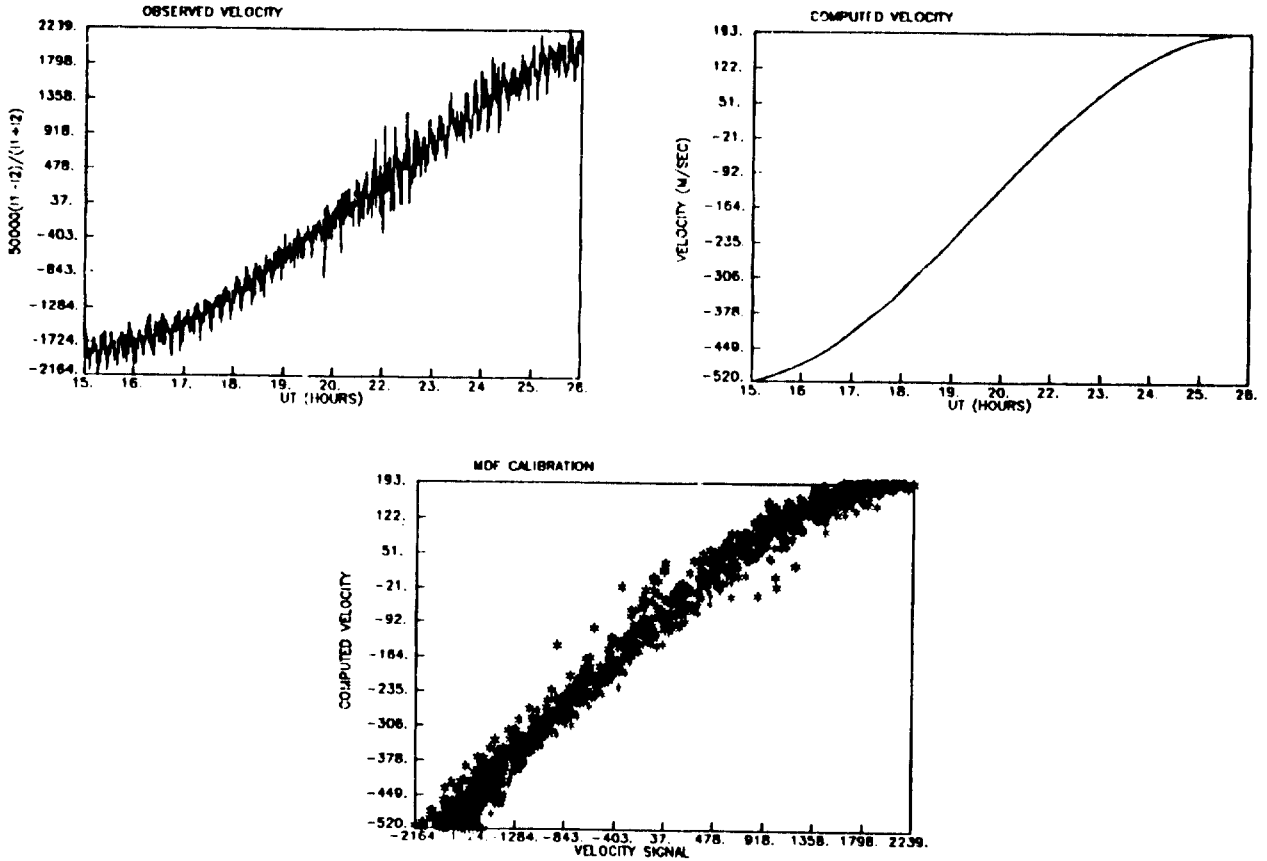

Figure 9. Re-Calibration Using Full-Disk Averages. The calibration procedure shown in Figure 8 is repeated here with Doppler signals obtained from full-disk averages of Dopplergrams taken on 27 July 1984. Here the departure from linearity is believed to be due to time-varying telluric contamination of the Na D2 line.

4. INITIAL DATA ANALYSIS

4.1 Spherical Harmonic Filtering

The next step in the data reduction sequence was the spherical harmonic filtering of the various time series of Dopplergrams. In order to carry out this filtering operation, we developed a computer program with which we could project spherical harmonic functions onto the planar 240 x 240 pixel grid of the CID camera images. Since the image registration program which translated all of the Dopplergrams from a given run to a common center also computed the radius of each solar image in pixels, we needed a program which was general enough to correct for the varying size of the solar image. In addition, we wanted a program which would allow for the position angle of the solar rotation axis and for the non-zero heliographic latitude of the sub-earth point on the solar disk. We also felt that it would be desirable for the harmonic generation scheme to be accurate up to ℓ-values of 1000 or more. Thus, the program which we developed can now generate fore-shortened spherical harmonics of the appropriate size and of any orientation.

Once the spherical harmonic generator had been developed, we next used its output to perform the spatial filtering. This was accomplished by dot-multiplying each Dopplergram with a given spherical harmonic on a pixel-by-pixel basis. This dot-multiplication corresponded to a double integration of the product of the Dopplergram and the harmonic. The output of this double integration was a separate filtered time series for each individual harmonic.

An example of such a filtered time series is shown here in Figure 10. In this Figure we show the detrended amplitude of the $\ell = 10$, $m = 10$ sectoral spherical harmonic as a function of time on July 27, 1984. Because of the non-linearity of the time-dependent calibration analysis for this July 27 observing run, as was shown in Figure 9, we did not in fact subtract off the computed sun-Earth velocity from each individual filtered Dopplergram. Instead, we decided to employ a simple third-order polynomial detrending analysis to remove the diurnal motion of the Earth from the filtered time series until we could correctly determine how to calibrate the July 27 dataset. Therefore, the time series displayed in Figure 10 has been both filtered and detrended.

Once the detrending analysis was complete, the information which remained in the filtered time series shown in Figure 10 was the amplitude which resulted from the beating together of all of the various solar oscillation modes having the spatial pattern given by the $\ell = 10$ sectoral harmonic, as well as some cross-talk from other, nearby sectoral and near-sectoral harmonics. (An analysis is now underway to determine more precisely the amount of cross-talk expected from such adjacent spherical harmonics.)

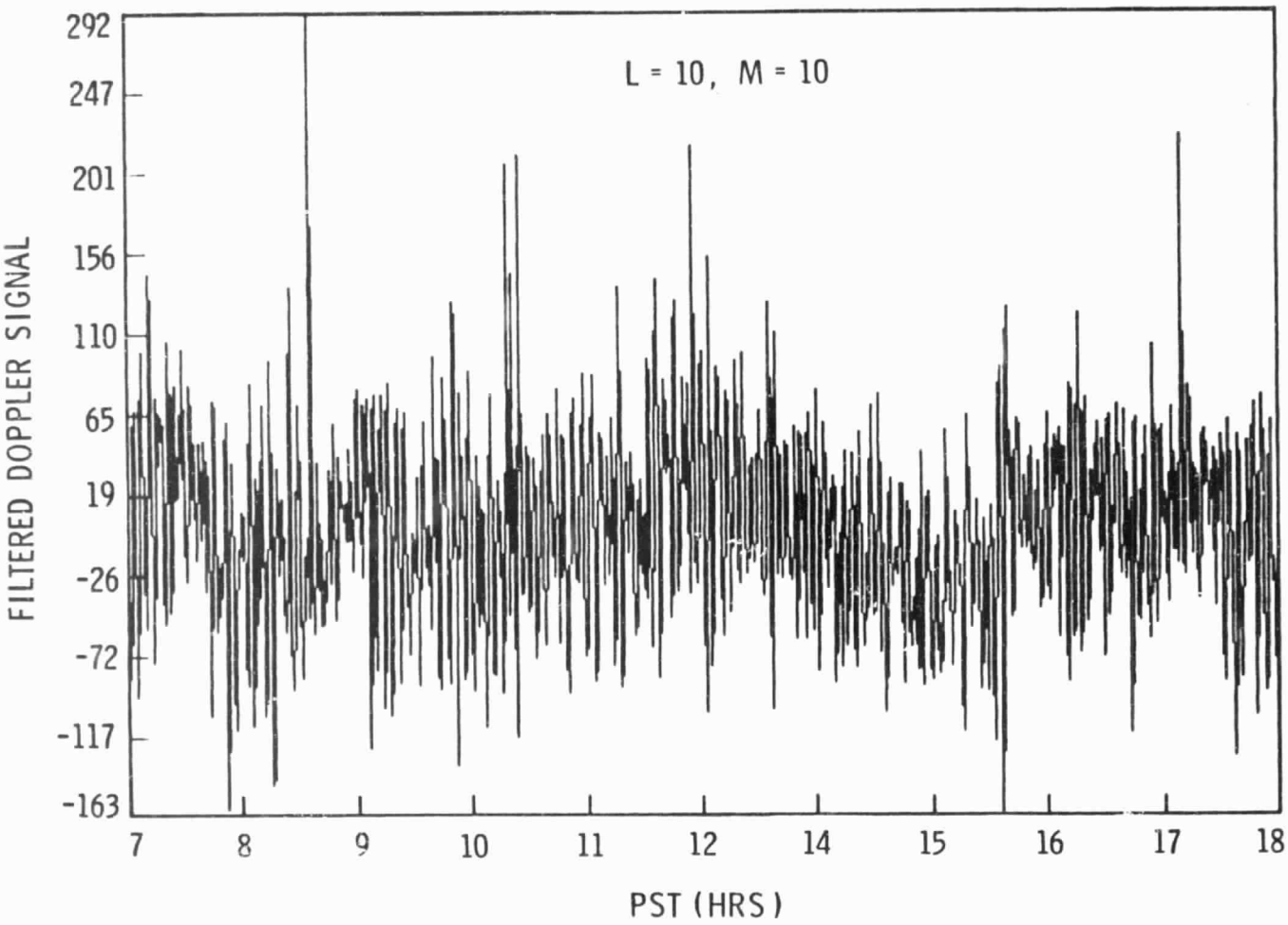

Figure 10. Filtered Doppler Signal. Here we show the result of filtering each Dopplergram obtained on 27 July 1984 with the sectoral harmonic having $\ell = 10$ and $m = 10$. The filtered time series shows the amplitude of this particular harmonic over the entire 11-hour observing day.

4.2 Power Spectral Computations

Once a filtered time series had been generated it was then a simple matter to employ a one-dimensional FFT program and compute the corresponding one-dimensional power spectrum. Three such power spectra from the July 27, 1984 run are shown in Figures 11, 12, and 13. Figure 11 shows the power spectrum which resulted from transforming the filtered time series shown in Figure 10. Therefore, the relative power levels of several $\ell = 10$ sectoral harmonics (along with some cross-talk from adjacent harmonics) are illustrated in this Figure. The power levels shown on the vertical axis are in arbitrary units since we had not employed the correct normalization constants at the time this spectrum was originally computed.

In Figure 11 the frequency unit employed is the circular frequency, ω instead of the linear frequency, ν. In these units the peak of the "5-minute" p-mode band is near $\omega = 0.020$ sec^{-1}. Due to the limited frequency resolution available from a single 11-hour observing run, the individual p-modes are not fully resolved in this spectrum. Nevertheless, the relatively low noise level of the MOF can be seen at frequencies between 0.004 and 0.016 sec^{1} and above 0.060 sec^{-1}.

At this time we should point out that the filters were operated without the benefit of any temperature stabilization scheme whatsoever. Furthermore, they were operated within the spectrograph chamber without the presence of any insulating material to shield them from ambient air temperature fluctuations. Lastly, the power supplies which controlled the heaters on the MOF cells, and hence the optical depth of the Na clouds within the cells, were not operated with any power regulation beyond that built into the supplies themselves. The rise in power level at frequencies below $w = 0.004$ sec^{-1} could be due in part to uncontrolled drifts in the power inputs to the cell heaters. (A closed-loop servo system which will control the temperature of the Na pits within the MOF cells to $\pm$ 0.1°C is now nearing completion and will soon be installed to test these ideas.)

Two more power spectral slices from the same day's data are illustrated here in Figures 12 and 13. In Figure 12 the power spectrum was completed from the dataset that had been filtered with the $\ell = m = 20$ sectoral harmonic, while in Figure 13 the $\ell = m = 40$ was used. The power levels are again not expressed in (m/sec)^2, although both power spectra should be normalized consistently with the spectrum of Figure 11. (That is to say that, while the absolute value of the normalization coefficients may not be correct, their relative values are. All of the factors which are ℓ- and m-dependent have been correctly included in the normalization coefficients already.) Note that while the noise level looks higher in Figures 12 and 13 than in Figure 11, the vertical scales are different. In fact, the absolute noise levels are quite similar in all three cases.

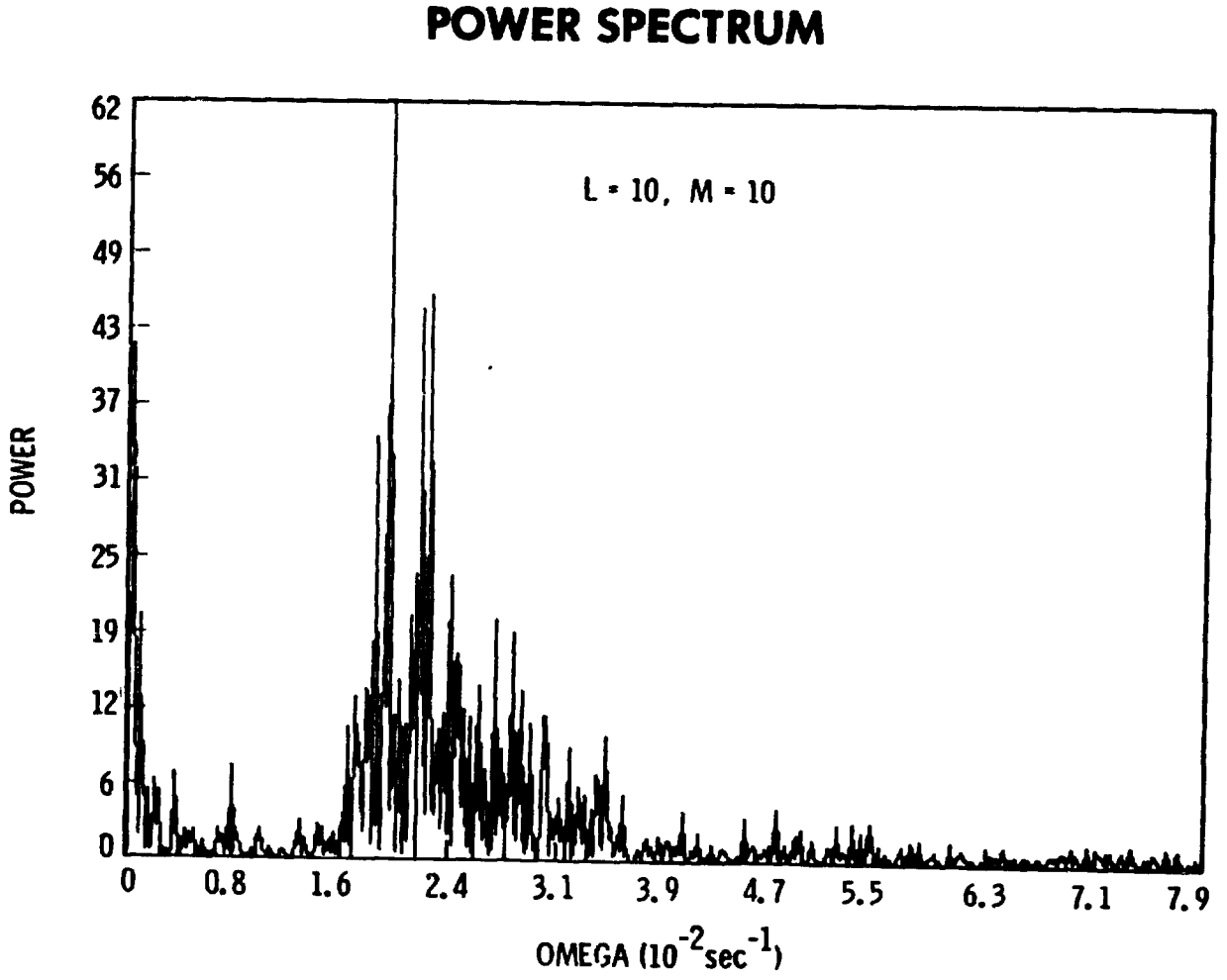

Figure 11. Power Spectral Slice. The one-dimensional power spectrum obtained by Fourier transforming the filtered time series displayed from Figure 10 is shown here. The power is plotted as a function of the circular frequency, ω, measured in units of 10^{-2} radians/sec.

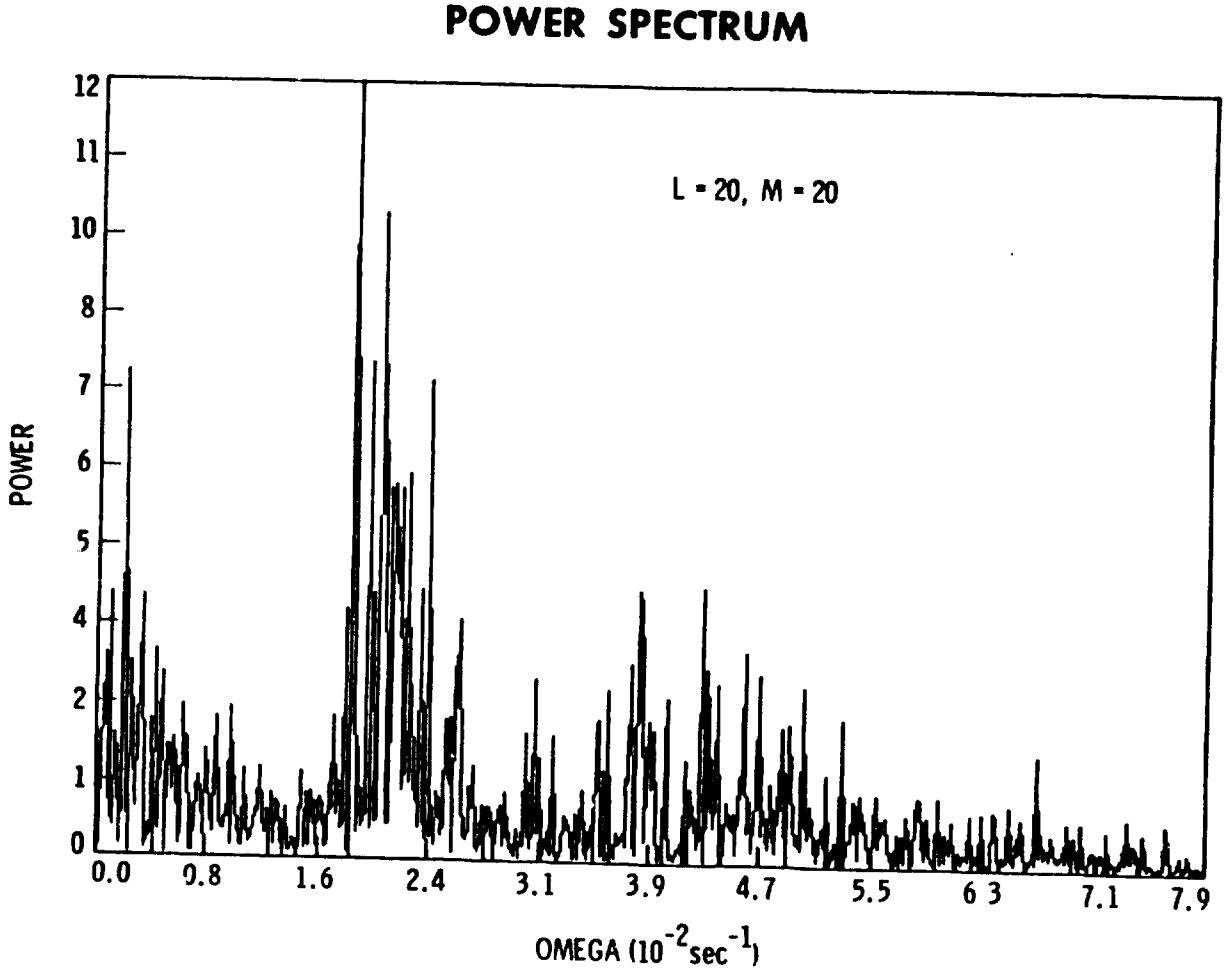

Figure 12. Same as Figure 11 except that this spectrum corresponds to the ℓ = 20, m = 20 sectoral harmonic.

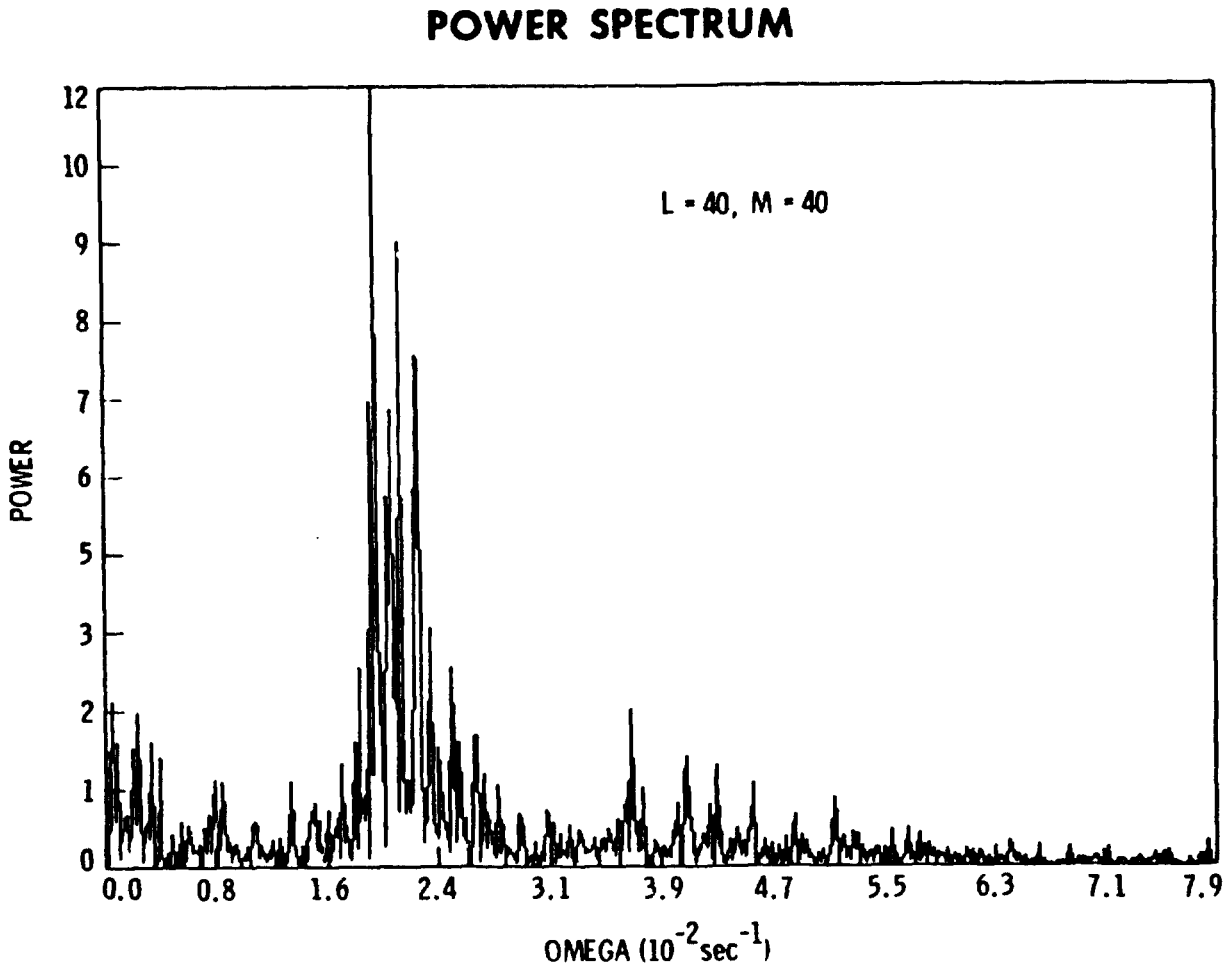

Figure 13. Same as Figures 11 and 12 except that this spectrum corresponds to the ℓ =40, m = 40 sectoral harmonic.

5. TASKS REMAINING

The tasks which remain in our processing of the summer 1984 data can be devided into three major areas. First, there are several difficulties with the preliminary processing of the data which we have already outlined above and which we must resolve before we can proceed. Second, there is the normous task of actually carrying out the analysis on the large number of data tapes which we have accumulated. Third, there is the scientific interpretation of the frequencies and frequency splittings which we will obtain from the power spectra.

There are four principal difficulties which comprise the first group of tasks. These are: 1) the problem with the non-linearity of the time-dependent velocity calibration analysis, 2) the search for possible spatial non-uniformities in the calibration coefficients, 3) the determination of the correct spherical harmonic normalization scheme, and 4) the re-coding of the spherical harmonic generation program and the spatial filtering program for our CSPI MAP 300 and Mini-MAP array processors in order to cut their execution times down to a manageable level.

The actual production runs to be carried out in the second phase will include: 1) the registration and calibration of the individual Dopplergrams for many more days of observations, 2) the spatial filtering analysis, 3) the time-synchronization of the filtered time series for multi-day runs, 4) the application of gap-filling techniques for the nighttime data gaps, 5) the computation of the power spectra from these multi-day filtered time series, and 6) the determination of the modal frequencies from the resulting power spectra.

The key scientific analyses to be carried out include: 1) the computation of the absolute frequencies for all of the modes observed as a function of harmonic degree, 2) the comparison of these frequencies with the predictions of various solar models, 3) the computation of the modal frequency splittings introduced by solar rotation, 4) the inversion of the frequency splittings in order to measure internal solar rotation as a function of both depth and latitude, and 5) a comparison of the absolute frequencies and the frequency splittings with those from earlier epochs in order to search for possible time-dependent changes in the sun.

6. SUMMARY

We have presented a review of the acquisition and preliminary analysis of the most extensive set of imaging data yet obtained anywhere for the study of solar oscillations. We have outlined the unique aspects of the instrumentation which have made the acquisition of this much data possible. We have gone on to describe some currently-unresolved difficulties with the data (as well as methods

which will hopefully allow us to resolve these difficulties). And we have presented a few preliminary results from our analyses of only a small amount of the available data. Finally, we have outlined the tasks which remain to be completed in our analysis.

REFERENCES

Agnelli, G., Cacciani, A., and Fofi, M., "The MOF I: Preliminary Observations in the Na D Lines," Solar Physics, 44, 509, 1975.

Brown, T. M., these proceedings; also HAO preprint submitted to Nature, 1985.

Cacciani, A., Cimino, M., and Fofi, M., "Some Developments of the Magnetic Beam Absorption Filter," Solar Physics, 11, 319, 1970.

Cacciani, A., Croce, U., Fortini, T., and Torelli, M., "Searching for ℓ=1 Modes of Solar Oscillation," Solar Physics, 74, 543, 1981.

Cacciani, A., and Fofi, M., "The MOF II: Velocity Field Measurements," Solar Physics, 59, 179, 1978.

Cacciani, A., Fortini, T., and Torelli, M., "Na-light Flare Observations: McMath 13043-July 1974," Solar Physics, 67, 311, 1980.

Cacciani, A., and Rhodes, E. J., Jr., "The Magneto-Optical Filter, Working Principles and Recent Progress," in Solar Seismology from Space, R. K. Ulrich, ed., JPL Publication 84-84, 115, 1984.

Cimino, M. Cacciani, A., and Sopranzi, N., "A Sharp Band Resonance Absorption Filter," Applied Optics, 7, 1654, 1968a.

Cimino, M., Cacciani, A., and Sopranzi, N., "An Instrument to Measure Solar Magnetic Fields by an Atomic-Beam Method," Solar Physics, 3, 618, 1968b.

Deubner, F.-L., "Observations of Low Wavenumber Nonradial Eigenmodes of the Sun," Astronomy and Astrophysics, 44, 371, 1975.

Deubner, F.-L., Ulrich, R. K., and Rhodes, E. J., Jr., "Solar p-Mode Oscillations as a Tracer of Radial Differential Rotation," Astronomy and Astrophysics, 72, 177, 1979.

Rhodes, E. J., Jr., Cacciani, A., Blamont, J., Tomczyk, S., Ulrich, R. K., and Howard, R. F., "Evaluation of a Magneto-optical Filter and a Fabry-Perot Interferometer for the Measurement of Solar Velocity Fields from Space," in Solar Seismology From Space, R. K. Ulrich, ed., JPL Publication 84-84, 125, 1985.

Rhodes, E. J., Jr., Cacciani, A., Tomczyk, S., Ulrich, R. K., Blamont, J., Howard, R. F., Dumont, P., and Smith, E. J., "A Compact Dopplergraph/Magnetograph Suitable for Space-Based Measurements of Solar Oscillations and Magnetic Fields," in Advances in Space Research, 4, 103, 1984.

Rhodes, E. J., Jr., Howard, R. F., Ulrich, R. K., and Smith, E. J., "New Instrumentation for Solar Oscillation Measurements at Mt. Wilson Observatory," in Solar Instrumentation: What's Next?, R. B. Dunn, ed., Sacramento Peak Observatory Publication, p. 102, 1981.

Rhodes, E. J., Jr., Howard, R. F., Ulrich, R. K., and Smith, E. J., "A New System for Observing Solar Oscillations at the Mount Wilson Observatory, I. Design and Installation," Solar Physics, 82, 245, 1983.

Rhodes, E. J., Jr., Ulrich, R. K., and Simon, G. W., "Observations of Nonradial p-Mode Oscillations on the Sun," Ap.J., 218, 901, 1977.

ACKNOWLEDGEMENTS

The research reported herein could not have been accomplished without the assistance of the following individuals: Thomas Andrews, Thomas Bursch, Douglas Clay, and Thomas Thorpe, all of the Jet Propulsion Laboratory; John Boyden, Maynard Clark, and Harvey Crist of the Mount Wilson Observatory; Nick Magnone, Daniel McKenna, James Wilkie, and Bradley Wood of the U.C.L.A. Astronomy Department; and Jeffrey Mannan of the Orbis Corporation. We also wish to acknowledge the assistance of Mr. Enzo Zante of the Italian National Laboratory for Alternative Energy (ENEA) in Frascati who helped with the fabrication of the MOF cells. The portion of the work carried out at U.S.C. was supported in part by NASA Grant NAGW-13. The work at U.C.L.A. was supported in part by NASA Grant NAGW-472. The work carried out at the Jet Propulsion Laboratory of the California Institute of Technology, Pasadena, California, was conducted under contract with the National Aeronautics and Space Administration. The portion of the work conducted in Italy was supported by the Italian Consiglio Nazionale delle Ricerche (CNR) and by the Ministero della Pubblica Istruzione.